J|A|C|S
ARTICLES
Published on Web 02/17/2004

Multielectron Chemistry of Zinc Porphyrinogen: A Ligand-Based Platform for Two-Electron Mixed Valency

Julien Bachmann and Daniel G. Nocera*

Contribution from the Department of Chemistry, 6-335, Massachusetts Institute of Technology, 77 Massachusetts Avenue, Cambridge, Massachusetts 02139-4307

Received November 15, 2003; E-mail: nocera@mit.edu

Abstract: The synthesis, electronic structure, and oxidation−reduction chemistry of a homologous series of Zn(II) porphyrinogens are presented. The fully reduced member of the series, $[LZn]^{2-}$, was prepared in two steps from pyrrole and acetone. The compound undergoes consecutive two-electron, ligand-based, oxidations at +0.21 and +0.63 V vs NHE to yield $[L^{\Delta}Zn]$ and $[L^{\Delta\Delta}Zn]^{2+}$, which also have been independently prepared by chemical means. X-ray diffraction analysis of the redox intermediary, $[L^{\Delta}Zn]$, shows that the partly oxidized macrocycle is composed of a methylene-bridged dipyrrole that is doubly strapped to a two-electron oxidized dipyrrole bridged by a cyclopropane ring (L^{Δ}). The localization of two hole equivalents on the oxidized side of the porphyrinogen framework is consistent with a two-electron mixed valency formulation for the $[L^{\Delta}Zn]$ species. Electronic structure calculations and electronic spectroscopy support this formalism. Density functional theory computations identify the HOMO to be localized on the reduced half of the macrocycle and the LUMO to be localized on its oxidized half. As implicated by the energy level diagram, the lowest energy transition in the absorption spectrum of $[L^{\Delta}Zn]$ exhibits charge-transfer character. Taken together, these results establish the viability of using a ligand framework as a two- and four-electron/hole reservoir in the design of multielectron redox schemes.

Introduction

Mixed valency in molecular compounds is typically accommodated at metal centers whose formal oxidation states differ by a single electron.[1−4] In these complexes, reactivity is confined to *single-electron* oxidations and reductions of the constituent M^n and M^{n+1} centers, respectively.[5−10] Extrapolating from this one-electron formalism, we have shown that two-electron mixed valency of bimetallic cores provides entry into a *multielectron* oxidation−reduction chemistry. Redox cooperativity may be established between the individual metal centers of a $M^n\cdots M^{n+2}$ mixed-valent core; two-electron oxidations may be promoted at a M^{n+2} center and two-electron reductions at a M^n center. Our success in using $M^n\cdots M^{n+2}$ species to drive two- and four-electron transformations along ground- and excited-state pathways[11−14] establishes the utility of two-electron mixed valency as a useful design concept in the development of multielectron reaction schemes. Due to our interest in expanding multielectron redox chemistry, we have begun exploring new approaches to two-electron mixed valency.

Two-electron mixed valency in our studies has heretofore been restricted to a metal core. Metal-to-metal charge-transfer excitation[15−18] or internal disproportionation of a symmetric $M^{n+1}\cdots M^{n+1}$ bimetallic core will yield a $M^n\cdots M^{n+2}$ species.[11,13,19] For either approach, the ligand framework is crucial for stabilizing the two-electron mixed-valent core with respect to its symmetric congener,[11,13,20,21] but it is not directly involved in the redox chemistry. Nevertheless, the active participation of ligands in the redox transformations of some metal complexes[22−25] suggests the antithetical approach to two-electron

(1) Taube, H. *Angew. Chem., Int. Ed. Engl.* **1984**, *23*, 329−339.
(2) Creutz, C. *Prog. Inorg. Chem.* **1983**, *30*, 1−73.
(3) *Mixed Valency System: Applications in Chemistry, Physics and Biology*; Prassides, K., Ed.; Kluwer Academic: Dordrecht, 1991; NATO ASI Series C: Mathematical and Physical Sciences 343.
(4) Schatz, P. N. In *Inorganic Electronic Structure and Spectroscopy*; Solomon, E. I., Lever, A. B. P., Eds.; Wiley-Interscience: New York, 1999; Vol. 2, pp 175−226.
(5) Ito, T.; Hamaguchi, T.; Nagino, H.; Yamaguchi, T.; Kido, H.; Zavarine, I. S.; Richmond, T.; Washington, J.; Kubiak, C. P. *J. Am. Chem. Soc.* **1999**, 121, 4625−4632.
(6) Ito, T.; Hamaguchi, T.; Nagino, H.; Yamaguchi, T.; Washington, J.; Kubiak, C. P. *Science* **1997**, *277*, 660−663.
(7) Vahrenkamp, H.; Geiss, A.; Richardson, G. N. *J. Chem. Soc., Dalton Trans.* **1997**, 3643−3651.
(8) Balzani, V.; Juris, A.; Venturi, M.; Campagna, S.; Serroni, S. *Chem. Rev.* **1996**, *96*, 759−833.
(9) Kunkely, H.; Pawlowski, V.; Vogler, A. *Inorg. Chim. Acta* **1994**, *225*, 327−330.
(10) Vogler, A.; Osman, A. H.; Kunkely, H. *Coord. Chem. Rev.* **1985**, *64*, 159−173.
(11) Heyduk, A. F.; Macintosh, A. M.; Nocera, D. G. *J. Am. Chem. Soc.* **1999**, *121*, 5023−5032.
(12) Odom, A. L.; Heyduk, A. F.; Nocera, D. G. *Inorg. Chim. Acta* **2000**, *297*, 330−337.
(13) Heyduk, A. F.; Nocera, D. G. *J. Am. Chem. Soc.* **2000**, *122*, 9415−9426.
(14) Heyduk, A. F.; Nocera, D. G. *Science* **2001**, *293*, 1639−1641.
(15) Engebretson, D. S.; Zaleski, J. M.; Leroi, G. E.; Nocera, D. G. *Science* **1994**, *265*, 759−762.
(16) Engebretson, D. S.; Graj, E.; Leroi, G. E.; Nocera, D. G. *J. Am. Chem. Soc.* **1999**, *121*, 868−869.
(17) Pistorio, B. J.; Nocera, D. G. *Chem. Commun.* **1999**, 1831−1832.
(18) Cotton, F. A.; Nocera, D. G. *Acc. Chem. Res.* **2000**, *33*, 483−490.
(19) Heyduk, A. F.; Nocera, D. G. *Chem. Commun.* **1999**, 1519−1520.
(20) Manke, D. R.; Nocera, D. G. *Inorg. Chem.* **2003**, *42*, 4431−4436.
(21) Hsu, T. L. C.; Helvoigt, S. A.; Partigianoni, C. M.; Turró, C.; Nocera, D. G. *Inorg. Chem.* **1995**, *34*, 6186−6190.
(22) Davison, A.; Edelstein, N.; Holm, R. H.; Maki, A. H. *Inorg. Chem.* **1963**, *2*, 1227−1232.
(23) Pierpont, C. G.; Lange, C. W. *Prog. Inorg. Chem.* **1994**, *41*, 331−442
(24) Wang, K.; Stiefel, E. I. *Science* **2001**, *291*, 106−109.

mixed valency wherein a ligand framework, as opposed to a bimetallic core, is exploited as the electron/hole reservoir. To this end, we turned our attention to porphyrinogen[26] since it has been shown that one or two cyclopropane rings may be formed from C−C coupling between the α-carbons of neighboring pyrroles upon oxidation of the tetrapyrrole; this transformation effectively entails the storage of two or four hole equivalents in the macrocycle ring.[27−34] The redox chemistry of the porphyrinogen framework, however, has remained ill-defined, and thus a multielectron chemistry involving these compounds has escaped characterization. For instance, the measurement of simple reduction potentials is obviated by redox-active axial ligands and/or polynuclear copper and iron halide counteranions, which are present in most oxidized porphyrinogens prepared to date.

We now report the porphyrinogens of the element zinc. Due to the absence of redox-active central metal, counterions, and axial ligands, the oxidation−reduction chemistry of the porphyrinogen macrocycle has been unveiled by electrochemistry. The reduction potentials of the porphyrinogen provide a road map to the preparation and isolation of a homologous $[LM]^{2-}$, $[L^{\Delta}M]$, $[L^{\Delta\Delta}M]^{2+}$ series where $[L^{\Delta}]^{2-}$ and $L^{\Delta\Delta}$ are the two- and four-electron oxidized porphyrinogen frameworks, respectively. Structural and spectroscopic properties unique to the $L^{\Delta}Zn$ intermediary support a two-electron mixed-valent formulation for $[L^{\Delta}]^{2-}$. Our results establish the viability of using a ligand framework to design two-electron mixed valency and provide a benchmark for the development of a multielectron chemistry of porphyrinogens containing redox-active metals.

Experimental Section

Materials. Handling of all compounds, reactions, and preparation of analytical samples were carried out in an inert atmosphere using standard Schlenk, drybox, and vacuum-line techniques. Solvents were purchased from VWR Scientific Products and purified using a Braun solvent purification system or using standard solvent purification techniques.[35] Deuterated solvents were purchased from Cambridge Isotope Laboratories, degassed, dried, and distilled by procedures similar to those used for nonisotopically enriched solvents. Technical-grade ferrocenium tetrafluoroborate ($FcBF_4$) was purchased from Aldrich, dissolved in acetonitrile, and dried over calcium hydride at room temperature; the solvent was degassed, and the solid was precipitated with diethyl ether, collected by filtration, and dried in vacuo. Octamethylporphyrinogen, LH_4, was prepared according to standard procedures.[27] Other reagents were purchased from Aldrich or Alfa Aesar and used as received. Elemental analyses were conducted at H. Kolbe Mikroanalytisches Laboratorium (Mühlheim a. d. Ruhr, Germany). Electrospray mass spectrometric analyses were conducted at the Mass Spectrometry Facility at the University of Illinois at Urbana−Champaign with a ±0.2 uncertainty on *m*/*z*.

Synthesis of $Li_2(THF)_x[LZn]$. A 10.0 g (23.3 mmol) sample of LH_4 was dissolved in 200 mL of THF, and a 2.89 M hexane solution of BuLi (46.7 mmol) was added dropwise and under stirring followed by the dropwise addition of a 1.0 M hexane solution of $ZnEt_2$ (23.3 mmol). The light yellow solution was refluxed gently overnight, cooled to room temperature and then to −80 °C to induce crystallization of a white solid, which was separated from the pale orange supernatant by filtration. *Caution*: Solid material is pyrophoric when exposed to air. The white powder was dried in vacuo; its THF content varied from one assay to the next and was assessed by ^1H NMR and elemental analysis. Yield: 14.6 g (86% for $x = 3$). ^1H NMR (500 MHz, DMSO-d_6, 20 °C): δ 5.43 (s, 8H, pyrrole), 3.61 (m, 12H, THF-β), 1.77 (m, 12H, THF-α), 1.56 (br, 12H, Me), 1.26 (br, 12H, Me). $^{13}C[^1H]$ NMR (100.6 MHz, DMSO-d_6, 20 °C): δ 145.5 (pyrrole), 97.1 (pyrrole), 67.0 (THF-α), 42.2 (br, Me), 36.3 (*meso*-C), 26.3 (br, Me), 25.2 (THF-β). UV−vis−NIR (THF): λ_{max} < 230 nm. IR: ν_{max} (cm^{-1}) = 3083 m (pyrrole C−H), 1348 m, 1278 m, 1216 m, 1156 m, 1050 s, 888 m, 761 s, 725 s. Anal. Calcd for $C_{40}H_{56}Li_2N_4O_3Zn$ ($x = 3$): C, 66.71; H, 7.84; N, 7.78. Found: C, 66.57; H, 8.09; N, 7.86.

Synthesis of $[L^{\Delta\Delta}Zn](BF_4)_2$. $Li_2(THF)_x[LZn]$ (2.99 mmol) was dissolved in 50 mL CH_3CN, stirred at 25 °C for 5 min, and then evaporated and thoroughly dried in vacuo. The solid was then redissolved in 80 mL of CH_3CN and added dropwise over a 5 min period to a 20 mL CH_3CN solution of $FcBF_4$ (3.39 g, 11.97 mmol). The deep emerald green solution was stirred at 25 °C for 15 min. The solvent was evaporated to leave a solid residue, which was dried in vacuo and resuspended in 600 mL of CH_2Cl_2. The solution was stirred until a fine suspension of the solid was obtained. The mixture was refluxed for 5 min and filtered warm. The green filtrate was evaporated; the remaining solid was dried and resuspended in 500 mL of hexane, and the mixture was stirred for 1 h at 25 °C. The green solid containing $[L^{\Delta\Delta}Zn](BF_4)_2$ and $FcBF_4$ was separated from the yellow Fc solution by filtration and dried in vacuo. Residual $FcBF_4$ was removed by suspending the powder in 60 mL of boiling CH_2Cl_2 and slowly adding hexane dropwise until solid beige $[L^{\Delta\Delta}Zn](BF_4)_2$ separated from a green-blue supernatant. The solid was collected by filtration after the suspension was cooled and dried in vacuo. Solid $[L^{\Delta\Delta}Zn](BF_4)_2$ was obtained as a light cream powder. Yield: 44% (0.88 g). ^1H NMR (500 MHz, CD_3CN, 20 °C): δ 7.93 (d, 5.5 Hz, 4H, pyrrole), 7.00 (d, 5.5 Hz, 4H, pyrrole), 2.03 (s, 6H, Me), 1.88 (s, 6H, Me), 1.82 (s, 6H, Me), 1.81 (s, 6H, Me). UV−vis−NIR (CH_3CN): λ_{max} < 230 nm. IR: ν_{max} (cm^{-1}) = 3111 m (pyrrole C−H), 1573 m, 1261 w, 1150 s, 1062 s, 1019 s, 884 m, 814 s, 723 m. Anal. Calcd for $C_{28}H_{32}B_2F_8N_4Zn$: C, 50.68; H, 4.86; N, 8.44; Zn, 9.85. Found: C, 50.42; H, 4.95; N, 8.38; Zn, 9.65. (+)ESI-MS $(M - 2BF_4^-)^{2+}$ calcd for $C_{28}H_{32}N_4Zn$ *m*/*z* 244.1, found 244.3.

Synthesis of $[L^{\Delta}Zn]\cdot(CH_2Cl_2)_y$. $Li_2(THF)_x[LZn]$ (0.137 mmol) was dissolved in 2 mL of CH_3CN and stirred for 5 min at 25 °C. The solvent was evaporated, and to the remaining solid was added a 5 mL solution of CH_3CN containing an equivalent amount of $L^{\Delta\Delta}Zn(BF_4)_2$ (0.091 g, 0.137 mmol). The resulting orange solution was evaporated to dryness, and the solid residue was collected and resuspended in 3 mL of CH_2Cl_2. Insoluble $LiBF_4$ was filtered off, and the filtrate was evaporated, yielding $[L^{\Delta}Zn]$ as an orange powder, which was recrystallized from CH_2Cl_2/pentane solvent mixture and dried in vacuo. Orange needles of $[L^{\Delta}Zn(CH_3CN)]\cdot CH_2Cl_2$ suitable for X-ray diffraction analysis were obtained from a CH_2Cl_2 solution containing a trace amount of CH_3CN layered with pentane. The bulk product contained a variable amount of cocrystallized CH_2Cl_2 from one assay to the next, which was assessed by elemental analysis. Yield: 92% (0.134 g for $y = 0.65$). UV−vis−NIR (CH_3CN): λ_{max} < 230 nm, 430 nm (ϵ = 630 M^{-1} cm^{-1}). IR: ν_{max} (cm^{-1}) = 3090 w (pyrrole C−H), 1568 m, 1353 m, 1278 w, 1218 w, 1155 m, 1103 s, 1055 s, 891 w, 802 m, 771 w, 723 m. Anal. Calcd

(25) Herebian, D.; Bothe, E.; Neese, F.; Weyhermueller, T.; Wieghardt, K. *J. Am. Chem. Soc.* **2003**, *125*, 9116−9128 and references therein.
(26) Baeyer, A. *Chem. Ber.* **1886**, *19*, 2184−2185.
(27) Jubb, J.; Floriani, C.; Chiesi-Villa, A.; Rizzoli, C. *J. Am. Chem. Soc.* **1992**, *114*, 6571−6573.
(28) Piarulli, U.; Solari, E.; Floriani, C.; Chiesi-Villa, A.; Rizzoli, C. *J. Am. Chem. Soc.* **1996**, *118*, 3634−3642.
(29) De Angelis, S.; Solari, E.; Floriani, C.; Chiesi-Villa, A.; Rizzoli, C. *J. Am. Chem. Soc.* **1994**, *116*, 5691−5701.
(30) De Angelis, S.; Solari, E.; Floriani, C.; Chies-Villa, A.; Rizzoli, C. *J. Am. Chem. Soc.* **1994**, *116*, 5702−5713
(31) Floriani, C.; Floriani-Moro, R. In *The Porphyrin Handbook*; Kadish, K. M., Smith, K. M., Guilard, R., Eds.; Academic Press: San Diego, CA, 2000; Vol. 3, Chapter 25, pp 405−420.
(32) Crescenzi, R.; Solari, E.; Floriani, C.; Chiesi-Villa, A.; Rizzoli, C. *J. Am. Chem. Soc.* **1999**, *121*, 1695−1706.
(33) Floriani, C. *Chimia* **1996**, *50*, 608−611.
(34) Belanzoni, P.; Rosi, M.; Sgamellotti, A.; Bonomo, L.; Floriani, C. *J. Chem. Soc., Dalton Trans.* **2001**, 1492−1497.
(35) Armarego, W. L. F.; Perrin, D. D. *Purification of Laboratory Chemicals*, 4th ed.; Butterworth-Heinmann: Oxford, 1996.

for $C_{29.65}H_{33.3}Cl_{1.3}N_4Zn$ ($y = 0.65$): C, 63.12; H, 6.16; N, 10.28; Zn, 12.00. Found: C, 62.73; H, 5.89; N, 9.92; Zn, 12.43.

X-ray Crystal Structure of $[L^{\Delta}Zn(CH_3CN)]\cdot CH_2Cl_2$. A bright orange crystal of $0.20 \times 0.10 \times 0.04$ mm^3 dimension was coated with Paratone N oil and mounted on a glass fiber. X-ray diffraction data were collected at −80 °C on a Siemens diffractometer equipped with a CCD detector, using the Mo Kα radiation, selected by a graphite monochromator. The data were integrated to *hkl*-intensity and the final unit cell calculated using the SAINT v.4.050 program from Siemens. Solution and refinement were performed with the SHELXTL v.5.03 suite of programs developed by G. M. Sheldrick and Siemens Industrial Automation, 1995. The structure was solved by the Patterson method; the least-squares refinement converged normally (with hydrogen atoms placed at calculated positions using a standard riding model and refined isotropically).

Physical Measurements. UV−vis−NIR solution absorption spectra were recorded between 220 and 1800 nm on a Cary-17 spectrophotometer modified by On-Line Instrument Systems (OLIS) to include computer control or a Spectral Instruments 440 Model spectrophotometer. IR spectra of samples in Nujol mulls were collected on a Perkin-Elmer 2000 FTIR spectrometer. ^{1}H and ^{13}C NMR spectra were recorded at the MIT Department of Chemistry Instrumentation Facility (DCIF) on a Varian Inova-500 or a Bruker Avance-400 spectrometer at 20 °C. Electrochemistry was performed with a standard three-electrode configuration using a CV-50W potentiostat (Bioanalytical Systems). The working electrode was Pt, the auxiliary electrode was a Pt wire and the reference was an $Ag/AgNO_3$ electrode, which was externally referenced to the Fc^+/Fc couple ($E°(Fc^+/Fc) = 0.65$ V (in CH_3CN) and 0.69 V (in THF) vs NHE).[36]

Computational Methods. Time-dependent density functional theory calculations (TD-DFT)[37,38] were performed using the Amsterdam Density Functional (ADF2002.02) program[39,40] on a home-built Linux cluster comprising 60 Intel Xeon processors organized in groups of 12 running in parallel at 2 GHz. The generalized gradient approximation was used as implemented in ADF by the LB94 functional,[41] allowing an accurate description of the asymptotic density behavior. A basis set of quadruple-ζ Slater-type functions augmented by triple polarization (ET-QZ3P) was used for all atoms, without frozen core approximation. The geometry was set at that observed in the experimental crystal structure, with CH_2Cl_2 removed; spin restriction was applied. Ten excitation energies were computed by the Davidson procedure.[42] A static Kohn−Sham molecular orbital picture was first obtained by a preliminary single-point calculation at a less heavy level (GGA Becke88 for exchange,[43] Perdew−Wang91 for correlation,[44] with TZ2P with frozen cores), and its results are essentially identical to those of the time-independent SCF routine of the more involved TD-DFT calculation, except for an offset of the orbital absolute energy scale. Therefore, the Kohn−Sham molecular orbital diagram and orbital pictures presented are those yielded by the Becke-PW91c/TZ2P single-point computation. Orbitals were visualized using the Molekel v.4.2 Linux-mesa software.[45,46]

Scheme 1

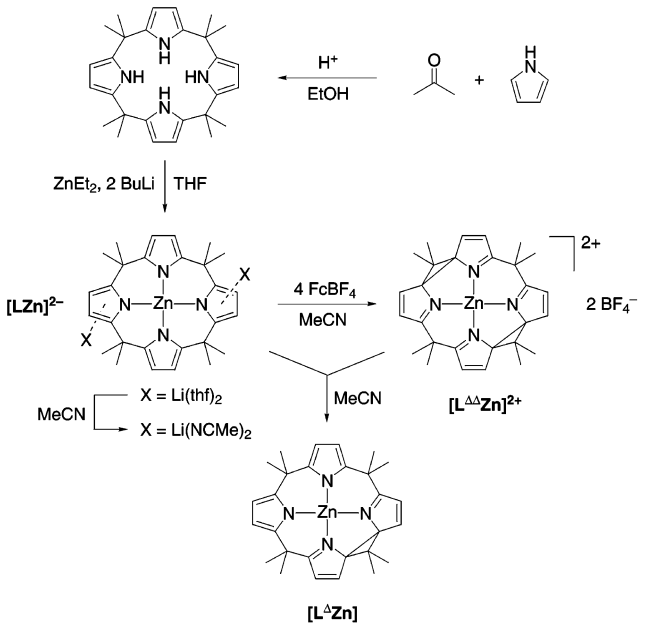

Results and Discussion

Synthesis and Redox Chemistry. The synthesis of the homologous zinc porphyrinogen series is outlined in Scheme 1. Zinc porphyrinogen $[LZn]^{2-}$ was prepared as its solvated lithium salt by direct reaction of the free ligand LH_4 with BuLi and $ZnEt_2$. A homoleptic dialkylzinc reagent allows for the convenient introduction of the Zn(II) ion in a single step from the free-base macrocycle. The *meso*-octamethyl-substituted derivative was chosen over the more common octaethyl derivative[47−56] because the latter is more prone to porphomethene and porphodimethene formation by oxidative elimination of ethylene.[31] We do note, however, that octamethyl derivatives are less soluble in typical organic solvents. Chair−chair interconversion of the macrocycle at room temperature is signified by distinct but broadened axial and equatorial CH_3 peaks in ^{1}H and ^{13}C NMR spectra of $Li_2(THF)_4[LZn]$. The fwhm of the ^{1}H methyl signal in DMSO-d_6 yields an exchange rate of 35 Hz, which increases to ∼350 Hz when the measurement is made in CD_3CN.

The fully oxidized member of the series, $[L^{\Delta\Delta}Zn]^{2+}$, is readily afforded from the oxidation of $[LZn]^{2-}$ in CH_3CN by 4 equiv of ferrocenium (Fc^+). The exact conditions (solvent and counterion) of this oxidation are crucial to its success since

(36) Connelly, N. G.; Geiger, W. E. *Chem. Rev.* **1996**, *96*, 877−910.
(37) van Gisbergen, S. J. A.; Kootstra, F.; Schipper, P. R. T.; Gritsenko, O. V.; Snijders, J. G.; Baerends, E. J. *Phys. Rev. A* **1998**, *57*, 2556−2571.
(38) Jamorski, C.; Casida, M. E.; Salahub, D. R. *J. Chem. Phys.* **1996**, *104*, 5134−5147.
(39) te Velde, G.; Bickelhaupt, F. M.; van Gisbergen, S. J. A.; Fonseca Guerra, C.; Baerends, E. J.; Snijders, J. G.; Ziegler, T. *J. Comput. Chem.* **2001**, *22*, 931−967.
(40) Fonseca Guerra, C.; Snijders, J. G.; te Velde, G.; Baerends, E. J. *Theor. Chem. Acc.* **1998**, *99*, 391−403.
(41) van Leeuwen, R.; Baerends, E. J. *Phys. Rev. A* **1994**, *49*, 2421−2431.
(42) van Gisbergen, S. J. A.; Snijders, J. G.; Baerends, E. J. *Comput. Phys. Commun.* **1999**, *118*, 119−138.
(43) Becke, A. D. *Phys. Rev. A* **1988**, *38*, 3098−3100.
(44) Perdew, J. P.; Chevary, J. A.; Vosko, S. H.; Jackson, K. A.; Pederson, M. R.; Singh, D. J.; Fiolhais, C. *Phys. Rev. B* **1992**, *46*, 6671−6687.
(45) Flükiger, P.; Lüthi, H. P.; Portmann, S.; Weber, J. Molekel v.4.2/3; Swiss Center for Scientific Computing: Manno, Switzerland, 2000−2002.
(46) Portmann, S.; Lüthi, H. P. *Chimia* **2000**, *54*, 776−770.
(47) Floriani, C.; Floriani-Moro, R. In *The Porphyrin Handbook*; Kadish, K. M., Smith, K. M., Guilard, R., Eds.; Academic Press: San Diego, CA, 2000; Vol. 3, Chapter 24, pp 385−403.
(48) Bonomo, L.; Solari, E.; Scopelliti, R.; Floriani, C. *Chem. Eur. J.* **2001**, *7*, 1322−1332.
(49) Bonomo, L.; Dandin, O.; Solari, E.; Floriani, C.; Scopelliti, R. *Angew. Chem., Int. Ed.* **1999**, *38*, 914−915.
(50) Bonomo, L.; Solari, E.; Floriani, C.; Chiesi-Villa, A.; Rizzoli, C. *J. Am. Chem. Soc.* **1998**, *120*, 12972−12973.
(51) Bonomo, L.; Solari, E.; Latronico, M.; Scopelliti, R.; Floriani, C. *Chem. Eur. J.* **1999**, *5*, 2040−2047.
(52) Bonomo, L.; Solari, E.; Martin, G.; Scopelliti, R.; Floriani, C. *Chem. Commun.* **1999**, 2319−2320.
(53) Campazzi, E.; Solari, E.; Scopelliti, R.; Floriani, C. *Chem. Commun.* **1999**, 1617−1618.
(54) Korobkov, I.; Aharonian, G.; Gambarotta, S.; Yap, G. P. A. *Organometallics* **2002**, *21*, 4899−4901.
(55) Korobkov, I.; Gambarotta, S.; Yap, G. P. A. *Angew. Chem., Int. Ed.* **2002**, *41*, 3433−3436.
(56) Korobkov, I.; Gambarotta, S.; Yap, G. P. A. *Angew. Chem., Int. Ed.* **2003**, *42*, 814−818.

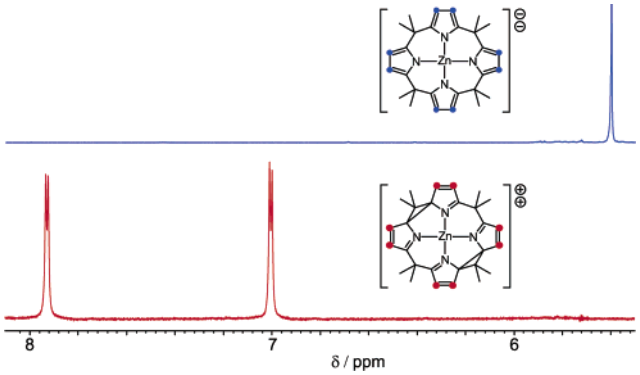

Figure 1. Pyrrole region of the ^{1}H NMR (CD_3CN, 500 MHz) spectra of $Li_2(THF)_x[LZn]$ (top) and $[L^{\Delta\Delta}Zn](BF_4)_2$ (bottom).

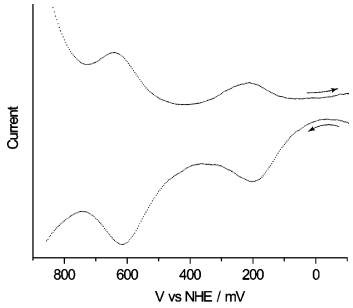

Figure 2. Differential pulse voltammograms recorded on a THF solution of $Li_2(THF)_x[LZn]$ (10^{-4} M) and Bu_4NPF_6 (0.01 M): scan rate 20 mV/s, pulse amplitude 50 mV, sample width 17 mV, pulse width 50 ms, pulse period 200 ms, quiet time 2 s.

$[L^{\Delta\Delta}Zn]^{2+}$ is extremely sensitive to radical oxidative elimination of the *meso*-alkyl substituents. The symmetry lowering attendant to cyclopropane ring formation is plainly evident in the ^{1}H NMR spectrum of $[L^{\Delta\Delta}Zn]^{2+}$ shown in Figure 1. The single pyrrole peak of $[LZn]^{2-}$ splits into two doublets, and the two methyl peaks split into four singlets. In addition, the large downfield shift of the pyrrole signals is indicative of increased conjugation upon macrocycle oxidation. In support of this contention, the proton resonances on porphyrins appear at values similar to those observed here. Cyclopropane formation is also apparent in the IR spectrum. The C−H stretching vibrations at 3083 cm^{-1} for the pyrrole rings of $[LZn]^{2-}$ shift to 3111 cm^{-1} in $[L^{\Delta\Delta}Zn]^{2+}$. New bands appear at 1050−1150 and 810 cm^{-1}, which we ascribe to the cyclopropane ring;[57] in addition, a band at 1575 cm^{-1} also appears upon oxidation that is consistent with a C═N stretching vibration of the oxidized pyrrole.

The redox transformations used in the preparative sequence of Scheme 1 are substantiated by direct electrochemical measurements. Figure 2 shows the differential pulse voltammogram measured on a THF solution of $[LZn]^{2-}$. Two waves are observed at +0.21 and +0.63 V vs NHE. The same DPV waves are obtained when solutions of $[L^{\Delta\Delta}Zn]^{2+}$ are scanned in a cathodic direction. This result suggests that the intermediate chemical species between the fully reduced $[LZn]^{2-}$ and fully oxidized $[L^{\Delta\Delta}Zn]^{2+}$ endpoints is the stable $[L^{\Delta}Zn]$ species. Moreover, the cyclic voltammetric trace of the $[L^{\Delta\Delta}Zn]^{2+}/[L^{\Delta}Zn]$ couple (Figure S1) indicates that $[L^{\Delta}Zn]$ is a stable species in solution; plots of the cathodic and anodic currents

(57) *Handbook of Data on Common Organic Compounds*; Lide, D. R., Milne, G. W. A., Eds.; CRC Press: Boca Raton, FL, 1995; Vol. 1.

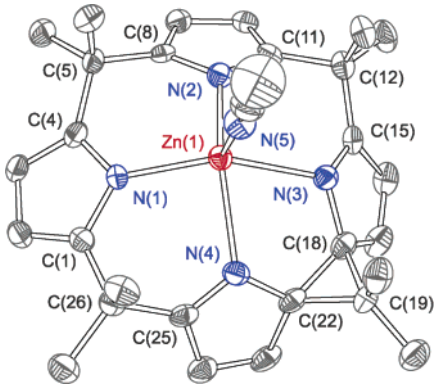

Figure 3. Solid-state structure of $[L^{\Delta}Zn(CH_3CN)]\cdot CH_2Cl_2$, with thermal ellipsoids drawn at the 50% probability level; hydrogen atoms, as well as a solvent CH_2Cl_2 molecule, are omitted for clarity.

vs $\nu^{1/2}$ (scan rate, ν = 50−600 mV s^{-1}) are linear. The $[L^{\Delta\Delta}Zn]^{2+}$ and $[LZn]^{2-}$ reduction potentials establish that $[L^{\Delta}Zn]$ can be obtained chemically by conproportionation. This is the case: $[L^{\Delta}Zn]$ is obtained in nearly quantitative yield by simply mixing equivalent amounts of $[L^{\Delta\Delta}Zn]^{2+}$ and $[LZn]^{2-}$. Unlike $Li_2(solv)_x[LZn]$ and $[L^{\Delta\Delta}Zn](BF_4)_2$, the neutral compound is very soluble in CH_2Cl_2, allowing us to obtain single crystals suitable for X-ray diffraction analysis.

Structural Chemistry. The structure of the $[L^{\Delta}Zn]$ macrocycle is shown in Figure 3. The central Zn(II) ion displays a distorted square pyramidal coordination geometry with the square base defined by the four pyrrole nitrogens of the macrocycle and the axial site capped with a nitrogen from coordinating CH_3CN. The central Zn(II) ion sits above the N_4 basal plane, forcing the macrocycle into a bowl conformation that is similar to the macrocyclic ring of LH_4 porphyrinogens (calix[4]pyrroles) hydrogen-bonded to an anion guest.[58−64] Crystallographic data are given in Table 1, and selected geometrical measurements are given in Table 2. The most striking structural characteristic of the macrocycle is that it effectively comprises the fused halves of a reduced and an oxidized porphyrinogen. The oxidized dipyrrole subunit is more sterically constrained due to the presence of the cyclopropane, which forces the coordinating nitrogens into closer proximity to each other. The N(3)−N(4) distance of the cyclopropane-bridged dipyrrole is only 2.69 Å, whereas the N(1)−N(2) distance between the methylene-bridged dipyrrole is 3.01 Å. The metrics associated with the cyclopropane ring are in line with those observed in monocyclopropane octaethylporphyrinogens of cobalt, nickel, and copper.[29,30] The cyclopropane is, within uncertainties, an equilateral triangle, with a $C^{\alpha}-C^{meso}-C^{\alpha}$ angle of 60.1(3)° and lengths of 1.544(7) and 1.534(6) Å for $C^{\alpha}-C^{meso}$ bond distances and 1.547(7) Å for the $C^{\alpha}-C^{\alpha}$ bond distance. This latter distance is significantly compressed relative to the 2.54 Å distance between the C^{α} of the pyrroles on the opposite side of the macrocycle. The presence of a cyclopropane ring causes changes in the $N-C^{\alpha}$ distances as well. Those of the pyrroles on the reduced side of the macrocycle are equivalent ($d(N-C^{\alpha})$ = 1.377 ± 0.008 Å), whereas the oxidized pyrroles exhibit a marked asymmetry arising from single-bond ($d(N-C^{\alpha})$ = 1.442 ± 0.003 Å) and double-bond ($d(N-C^{\alpha})$ = 1.299 ± 0.002 Å) alternation.

The difference between the two halves of the macrocycle is also reflected in the primary coordination sphere of the Zn(II)

Table 1. Summary of X-ray Crystallography Data for $[L^{\Delta}Zn(CH_3CN)]\cdot CH_2Cl_2$

empirical formula	$C_{31}H_{37}Cl_2N_5Zn$
formula weight	615.93
T (K)	193(2)
λ (Å)	0.71073
crystal system	triclinic
space group	$P\bar{1}$
a (Å)	10.3850(8)
b (Å)	10.6155(9)
c (Å)	14.4068(12)
α (deg)	81.8540(10)
β (deg)	85.3500(10)
γ (deg)	73.086(2)
V (Å^3)	1502.9(2)
Z	2
ρ_{calcd} (g/cm^3)	1.361
crystal size (mm^3)	0.20 × 0.10 × 0.04
abs coeff (mm^{-1})	1.024
F(000)	644
θ range for data collection	2.44 to 23.25°
limiting indices	$-11 \le h \le 11$, $-11 \le k \le 6$, $-15 \le l \le 15$
no. of reflections collected	6891
no. of indicative reflections (R_{int})	4253 (0.0627)
completeness to $\theta = 23.25°$	98.6%
refinement method	full-matrix least-squares on F^2
data/restraints/parameters	4253/0/362
$R1$,[a] $wR2$[b] [$I > 2\sigma$]	0.0609, 0.1140
$R1$,[a] $wR2$[b] (all data)	0.0861, 0.1227
GOF[c] on F^2	1.071
extinction coefficient	0.0000(8)
largest difference peak and hole	0.641 and −0.469 e/Å^3

[a] $R1 = \Sigma||F_o| - |F_c||/\Sigma|F_o|$. [b] $wR2 = (\Sigma(w(F_o^2 - F_c^2)^2)/\Sigma(w(F_o^2)^2))^{1/2}$. [c] GOF $= (\Sigma\, w(F_o^2 - F_c^2)^2/(n - p))^{1/2}$ where n is the number of data and p is the number of parameters refined.

ion. The reduced dipyrrole half of the macrocycle appears to formally carry the negative charge of the dianionic ligand, as evidenced by compressed Zn−N bond lengths of 2.029 and 2.019 Å. Conversely, the oxidized, neutral half of the macrocycle displays longer Zn−N bond lengths of 2.212(4) and 2.237(4) Å; these distances are even longer ($\Delta d \approx 0.1$ Å) than those observed in neutral chelating bipyridine complexes of Zn(II).[65] The structural differences between the two sides of the porphyrinogen very clearly implicate a two-electron mixed-valence formalism for the macrocycle composed of two ligands within one, in which a dipyrrole is doubly strapped to a two-electron oxidized dipyrrole.

Electronic Structure. The two-electron mixed-valent nature of the $[L^{\Delta}]^{2-}$ macrocycle is evident in Figure 4, which shows the absorption spectra for the three compounds of the series. The spectra of $[L^{\Delta\Delta}Zn]^{2+}$ and $[L^{\Delta}Zn]$ are recorded in CH_3CN, whereas that of $[LZn]^{2-}$ is recorded in THF. This choice of solvents is dictated by the solution chemistry of the compounds. Acetonitrile $[LZn]^{2-}$ solutions exhibit a near-UV absorption band whose energy ($\lambda_{max} = 300-400$ nm) and intensity are concentration dependent; the band vanishes in the spectrum of the compound in THF. We attribute this behavior to cation-promoted aggregation of the macrocycle, which is suppressed when the Li^+ cation is solvated by THF. Consistent with this tenet, similar behavior was reproduced for the absorption spectrum of the Li^+ salt of deprotonated pyrrole (prepared by reacting pyrrole with butyllithium). In the case of $[L^{\Delta\Delta}Zn]^{2+}$ and $[L^{\Delta}Zn]$, the insufficient stability of the compounds in THF prevents us from measuring absorption data in this solvent. However, CH_3CN is a viable solvent for these compounds since they do not possess any countercations.

The absorption profiles of the fully reduced and oxidized members, $[LZn]^{2-}$ and $[L^{\Delta\Delta}Zn]^{2+}$, are similar, unremarkable and in accordance with their colorless appearance. A rising absorption into the UV spectral region is consistent with the presence of a strongly absorbing $\pi \rightarrow \pi^*$ transition of pyrrole at high energy ($\lambda_{max} = 208$ nm).[66] The UV spectral region of $[L^{\Delta}Zn]$ is also dominated by the rising absorption edge of the $\pi \rightarrow \pi^*$ transition of the constituent pyrroles. However, the color of the intermediate is distinct from its endpoint series members. Whereas $[LZn]^{2-}$ and $[L^{\Delta\Delta}Zn]^{2+}$ are white and pale beige solids, $[L^{\Delta}Zn]$ is intensely orange. This color arises from a broad absorption whose observed maximum occurs at 430 nm in CH_3CN. We ascribe this solvent-dependent (vide infra) absorption to an intra-porphyrinogen charge transfer (ICT) from the reduced dipyrrole half of the macrocycle to its two-electron oxidized dipyrrole neighbor.

The ICT character of $[L^{\Delta}Zn]$ was examined further by DFT calculations. Figure 5 displays the color-coded energy levels and representations of the frontier Kohn−Sham molecular orbitals. We note that the Kohn−Sham orbitals differ from those derived from a Hartree−Fock (HF) formalism by the inclusion of the exchange-correlation energy;[67] however, comparative analysis establishes that the shapes and symmetries of the Kohn−Sham orbitals accord well with those calculated by more traditional HF and extended Hückel approximations,[68,69] and indeed these orbitals have found widespread use in electronic structure descriptions.[70−74] The most striking feature of the energy level diagram is the clear-cut division of orbital parentage between oxidized and reduced sides of the ligand. The highest-energy occupied molecular orbitals are localized on the reduced half of the macrocycle, whereas the lowest-energy unoccupied orbitals are localized on the oxidized half of the porphyrinogen. The Zn d-orbitals lie very deep in the MO diagram (HOMO-29 to HOMO-33) and effectively do not contribute to the frontier MOs. The HOMO to HOMO-3 are the e_1''-type orbitals (based

(58) Gale, P. A.; Sessler, J. L.; Král, V.; Lynch, V. J. *J. Am. Chem. Soc.* **1996**, *118*, 5140−5141.
(59) Anzenbacher, P., Jr.; Jursíková, K.; Lynch, V. M.; Gale, P. A.; Sessler, J. L. *J. Am. Chem. Soc.* **1999**, *121*, 11020−11021.
(60) Miyaji, H.; Sato, W.; Sessler, J. L. *Angew. Chem., Int. Ed.* **2000**, *39*, 1777−1780.
(61) Sessler, J. L.; Anzenbacher, P., Jr.; Miyaji, H.; Jursíková, K.; Bleasdale, E. R. Gale, P. A. *Ind. Eng. Chem. Res.* **2000**, *39*, 3471−3478.
(62) Blás, J. R.; Márquez, M.; Sessler, J. L.; Luque, J.; Orozco, M. *J. Am. Chem. Soc.* **2002**, *124*, 12796−12805.
(63) Nielsen, K. A.; Jeppesen, J. O.; Levillain, E.; Becher, J. *Angew. Chem., Int. Ed.* **2003**, *42*, 187−191.
(64) Yoon, D.-W.; Hwang, H.; Lee, C.-H. *Angew. Chem., Int. Ed.* **2002**, *41*, 1757−1759.
(65) Liu, M.; Arora, S. K. *Acta Crystallogr. C* **1993**, *49*, 372−374.
(66) Perkampus, H.-H. *UV−Vis Atlas of Organic Compounds*; VCH Verlagsgesellschaft: Weinheim, 1992.
(67) Kohn, W.; Becke, A. D.; Parr, R. G. *J. Phys. Chem.* **1996**, *100*, 12974−12980.
(68) Stowasser, R.; Hoffmann, R. *J. Am. Chem. Soc.* **1999**, *121*, 3414−3420.
(69) Hamel, S.; Duffy, P.; Casida, M. E.; Salahub, D. R. *J. Electron Spectrosc. Relat. Phenom.* **2002**, *123*, 345−363.
(70) Lehnert, N.; Neese, F.; Ho, R. Y. N.; Que, L., Jr.; Solomon, E. I. *J. Am. Chem. Soc.* **2002**, *124*, 10810−10822.
(71) Chen, P.; Root, D. E.; Campochiaro, C.; Fujisawa, K.; Solomon, E. I. *J. Am. Chem. Soc.* **2003**, *125*, 466−474.
(72) Chisholm, M. H.; Gallucci, J.; Hadad, C. M.; Huffman, J. C.; Wilson, P. J. *J. Am. Chem. Soc.* **2003**, *125*, 16040−16049.
(73) Gray, T. G.; Rudzinski, C. M.; Meyer, E.; Holm, R. H.; Nocera, D. G. *J. Am. Chem. Soc.* **2003**, *125*, 4755.
(74) Gray, T. G.; Rudzinski, C. M.; Meyer, E. E.; Nocera, D. G. *J. Phys. Chem.* **2004**, in press.

Table 2. Selected Geometric Lengths (Å) and Angles (deg) for $[L^{\Delta}Zn(CH_3CN)]\cdot CH_2Cl_2$[a]

bond distances (Å)							
Zn−N(1)	2.029(4)	N(1)−C(4)	1.369(6)	N(3)−C(18)	1.440(6)	C(18)−C(19)	1.544(7)
Zn−N(2)	2.019(4)	N(1)−C(1)	1.387(6)	N(4)−C(25)	1.298(6)	C(19)−C(22)	1.534(6)
Zn−N(3)	2.212(4)	N(2)−C(8)	1.379(6)	N(4)−C(22)	1.445(6)	C(18)−C(22)	1.547(7)
Zn−N(4)	2.237(4)	N(2)−C(11)	1.385(6)	C(4)−C(5)	1.520(7)		
Zn−N(5)	2.101(4)	N(3)−C(15)	1.301(6)	C(5)−C(8)	1.527(6)		
bond angles (deg)							
N(1)−Zn−N(2)	95.92(15)	N(1)−Zn−N(5)	106.44(16)	C(8)−N(2)−Zn	121.8(3)	C(29)−N(5)−Zn	175.0(4)
N(2)−Zn−N(3)	88.24(15)	N(2)−Zn−N(5)	107.77(16)	C(11)−N(2)−Zn	127.9(3)	C(4)−C(5)−C(8)	112.9(4)
N(1)−Zn−N(3)	149.71(15)	N(3)−Zn−N(5)	100.72(15)	C(15)−N(3)−Zn	122.7(3)	C(19)−C(18)−C(22)	59.5(3)
N(2)−Zn−N(4)	149.26(15)	N(4)−Zn−N(5)	100.36(15)	C(18)−N(3)−Zn	118.3(3)	C(22)−C(19)−C(18)	60.3(3)
N(1)−Zn−N(4)	87.64(14)	C(4)−N(1)−Zn	122.6(3)	C(25)−N(4)−Zn	120.8(3)	C(19)−C(22)−C(18)	60.1(3)
N(3)−Zn−N(4)	74.35(14)	C(1)−N(1)−Zn	128.2(3)	C(22)−N(4)−Zn	117.1(3)		

[a] Atom numbering scheme provided in Figure 3.

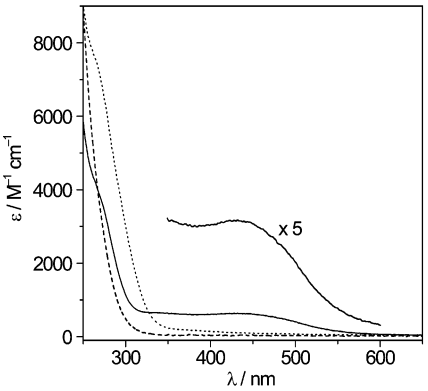

Figure 4. UV−visible absorption spectra of $Li_2(THF)_x[LZn]$ (− − −) in THF and $[L^{\Delta}Zn(CH_3CN)]$ (—) and $[L^{\Delta\Delta}Zn](BF_4)_2$ (- - -) in CH_3CN. The inset shows a magnification (×5) of the absorption profile of $[L^{\Delta}Zn(CH_3CN)]$ in the visible spectral region.

on a $C_5H_5^-$ (D_{5h}) reference) of the pyrroles on the reduced side of the porphyrinogen. An orbital pair arises from the bonding and antibonding interaction of orbitals on individual pyrroles along the $C^{\alpha}-C^{\alpha}$ axis of the dipyrrole subunit. The weak interaction between pyrrole subunits on the reduced side of the porphyrinogen, indicated by the small energy difference of 0.15 eV for bonding and antibonding linear combinations, is consistent with the long $C^{\alpha}\cdots C^{\alpha}$ distance. The MOs formed from the equivalent e_1''-type π orbital set of pyrroles on the oxidized half of the porphyrinogen also appear as pairs due to $C^{\alpha}-C^{\alpha}$ bonding and antibonding combinations. The HOMO-6/HOMO-5 orbitals are composed of e_1''-type orbitals that are effectively insulated from each other by the absence of electron density at C^{α}. HOMO-6/HOMO-5 are more stable than their e_1''-type counterparts on the reduced dipyrrole (ΔE = E(HOMO-6/HOMO-5) − E(HOMO-2/HOMO-3) ≈ −2 eV) due to the greater electronegative character of the oxidized half of the macrocycle. The other e_1''-type-derived MO pair on the oxidized pyrroles is displayed in Scheme 2 from an end-on perspective of the dipyrrole unit. The sp^3 character of C^{α} causes the pyrrole rings of the oxidized subunit to assume an orientation nearly perpendicular to the plane of the cyclopropane ring. This stereochemistry causes an antibonding interaction between $p\pi$(pyrrole) and $p\sigma$(cyclopropane bridgehead) orbitals that is sufficiently destabilizing to place the e_1''-type MOs at the LUMO/LUMO + 1 position. As a result, the frontier MO set exhibits a LUMO localized on the oxidized half of the porphyrinogen and a HOMO localized on the reduced half of the porphyrinogen. The MO diagram therefore nicely accounts for the ICT assignment to the lowest energy absorption band of $[L^{\Delta}Zn]$. As implicated by the energy level diagram, several ICT transitions may arise within this manifold, qualitatively explaining the breadth of the charge-transfer transition.

Other notable highlights of the MO diagram include the HOMO-9, which is framed in Figure 5. The orbital embodies the antithetical interaction that leads to the LUMO. Specifically, the e_1''-type orbitals on the oxidized dipyrroles are bonding with respect to the cyclopropane bridgehead, engendering a very stable MO. The e_2''-type orbitals of the pyrroles contribute to unoccupied MOs that lie at higher energy. On the oxidized dipyrrole half of the porphyrinogen, the e_2''-type-derived MOs are energetically proximate to the LUMO (LUMO + 5 to LUMO + 8); the MOs involving the e_2''-type orbitals on the reduced half of the porphyrinogen are very high in energy and not shown. The MOs involving the CH_3CN are unremarkable and have little effect on the structure and spectroscopy of the $[L^{\Delta}Zn]$ complex.

Juxtaposed reduced and oxidized dipyrrole subunits engender a large dipole moment in the ground electronic state of the $[L^{\Delta}Zn]$ complex. This is reflected in the Mulliken charge analysis of the porphyrinogen framework. The N atoms of the oxidized dipyrrole bear significantly less negative charge (−0.42 charge units) than those of the reduced dipyrrole (−0.50 and −0.51 charge units, respectively), although all pyrrole N atoms are clearly more negative than that of the axially ligated acetonitrile N (−0.23). A dipole moment of 11.9 D is calculated for the ground-state molecule, though we acknowledge that this value is tenuous inasmuch as the calculation has been performed for a gas-phase species. Notwithstanding, the calculation is categorically predictive. The large dipole in the ground state should be alleviated by the electron redistribution accompanying ICT excitation. In a limiting resonance form of the ICT excited state of $[L^{\Delta}Zn]$, the dipole will be annihilated.

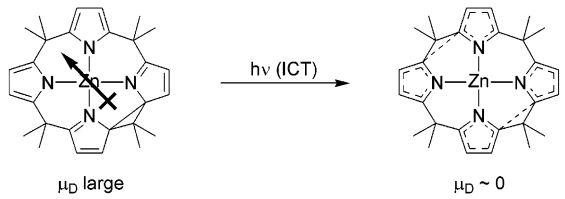

Polar solvents should stabilize the ground state of $[L^{\Delta}Zn]$ relative to its lowest energy ICT excited state. As the static

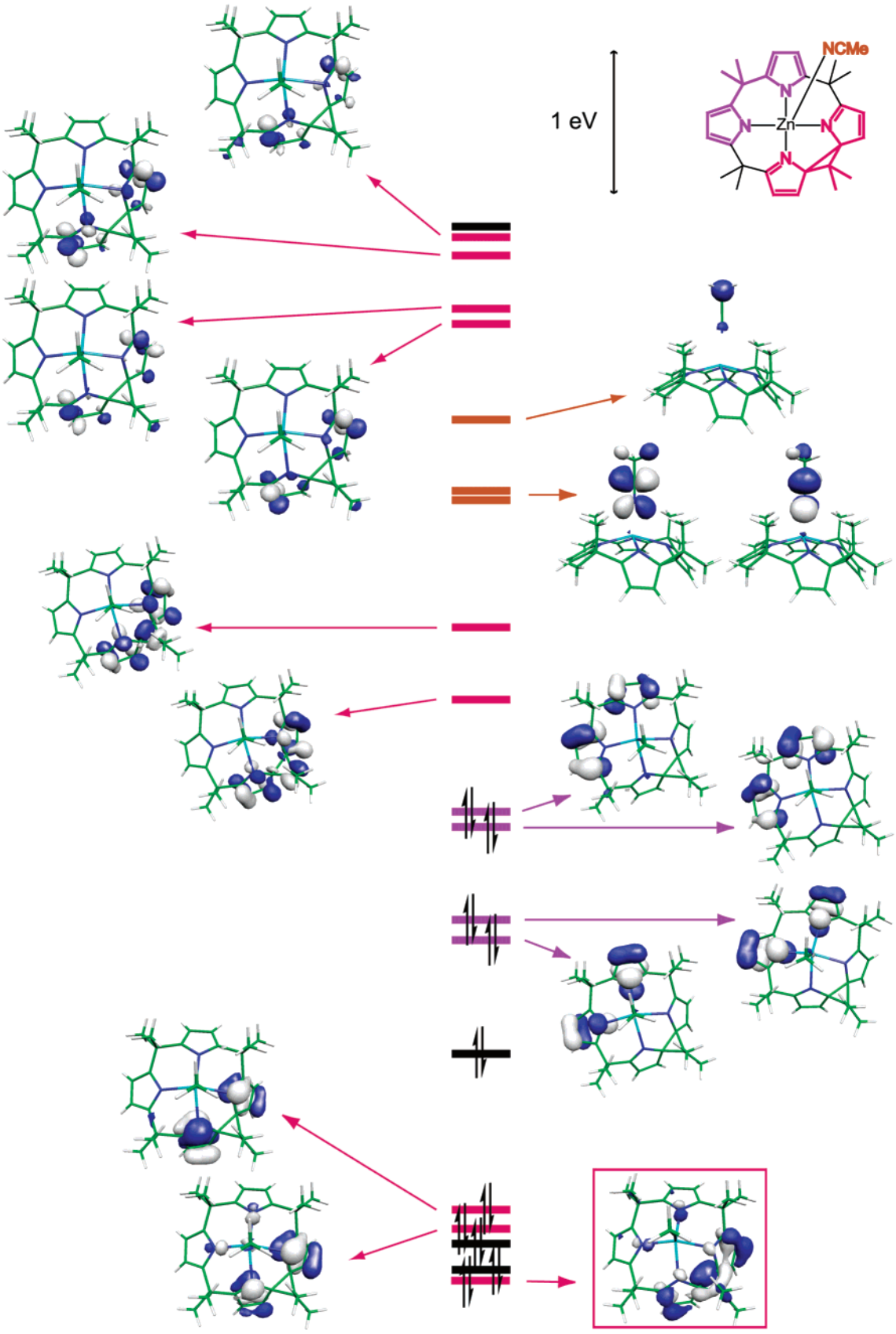

Figure 5. Partial Kohn−Sham MO diagram of [L^{A}Zn(CH_3CN)]. Orbitals located in particular regions of the molecule are color-coded (the oxidized half of the macrocycle in pink, the reduced half in lilac, and the coordinated CH_3CN in orange), and σ-type orbitals delocalized over most of the molecule are in black. Orbitals are drawn as isodensity surfaces encompassing 0.95 e (of each spin). The HOMO-9, framed in pink, carries most of the $C^{\alpha}-C^{\alpha}$ bonding interaction of the cyclopropane ring.

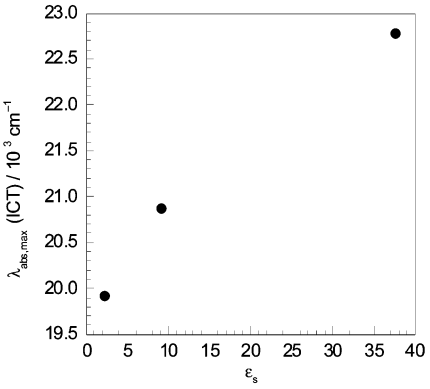

Figure 6. Solvent dependence (ϵ_s = solvent static dielectric constant) of the absorption maximum of the ICT transition of [L^{Δ}Zn], determined by a Gaussian fit of the lowest energy band. The spectra were recorded in CH_3CN, CH_2Cl_2, and toluene (in which [L^{Δ}Zn] is very soluble, very soluble, and sparingly soluble, respectively).

Scheme 2

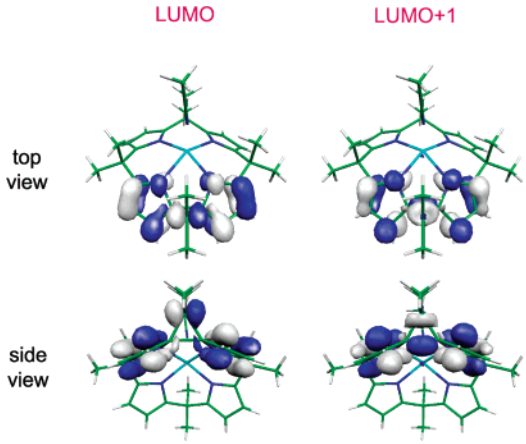

dielectric constant of the solvent is decreased, the ground state should be destabilized, and thus the HOMO−LUMO gap should decrease. Atypical of most charge-transfer transitions, the energy of the ICT transition of [L^{Δ}Zn] should therefore blue-shift as the polarity of the solvent increases. The data shown in Figure 6 validate this prediction.

Conclusions

The oxidation−reduction chemistry of a porphyrinogen framework has been unveiled by synthesizing the macrocycle in the absence of redox-active metal, axial ligand, and counterions. The Zn(II) porphyrinogen reacts in two-electron steps with the concomitant formation of a C−C bond between the α carbons of adjacent pyrroles; each cyclopropane thus formed is a two-equivalent hole reservoir for the porphyrinogen framework. By spanning fully reduced $[LZn]^{2-}$ and oxidized $[L^{\Delta\Delta}Zn]^{2+}$ brethren, [L^{Δ}Zn] sustains an overall four-electron transformation. Structural and spectroscopic properties show that the [L^{Δ}Zn] macrocycle is composed of a dipyrrole doubly strapped to a two-electron oxidized dipyrrole neighbor. From this standpoint, the [L^{Δ}Zn] species may be described formally as the two-electron mixed-valent intermediary of the homologous multielectron series.

This formulation of two-electron mixed valency for porphyrinogens is further emphasized in Scheme 3, which parallels the oxidation states of the Zn(II) porphyrinogen macrocycles

Scheme 3

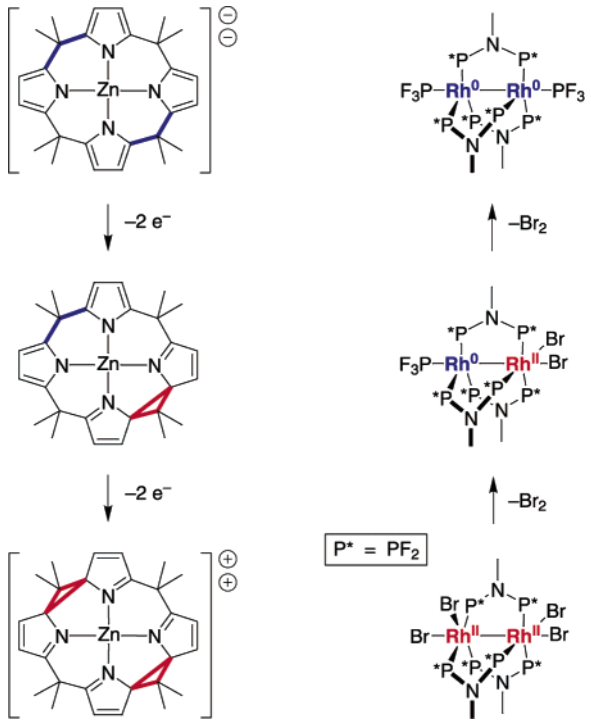

to those of the dirhodium centers that we have stabilized with the bis(difluorophosphino)methylamine ligand.[11] Several similarities between ligand-based and metal-based approaches to two-electron mixed valency are evident. For both approaches, (1) the two-electron mixed-valent intermediate is the linchpin that couples the two-electron chemistry of the individual redox centers (dipyrroles in the case of porphyrinogen, rhodium centers in the case of the bimetallic complex), (2) the two-electron mixed-valent compound is the structural composite of the symmetric oxidized and reduced congeners, and (3) the frontier molecular orbitals and corresponding lowest energy electronic transitions are confined to the two-electron mixed-valent core.[75] Despite these similarities, the ligand-based approach to two-electron mixed valency differs from that of a metal-based approach in one important aspect. Because coordination geometry is inextricably linked to metal oxidation state, two-electron/hole storage in the metal-based approach must be accompanied by alterations of the primary coordination sphere. Conversely, in the approach described here, two-electron/hole storage occurs in the macrocycle periphery, decoupled from the acid−base chemistry of the metal. This orthogonalization between redox storage and small-molecule coordination sites offers a new design element for using two-electron mixed valency to promote multielectron reactivity. Small-molecule multielectron activation at a porphyrinogen platform will be contingent on relaying redox equivalents from the macrocycle to a redox-active central metal. Studies aimed at exploring such processes are currently underway.

Acknowledgment. This work was supported by a grant from the National Science Foundation (CHE-0132680). J.B. gratefully acknowledges MIT for a predoctoral Presidential Fellowship and the Shell Oil Company for a graduate research fellowship.

(75) For the $Rh^0-Rh^{II}X_2$ complex, see: Kadis, J.; Shin, Y.-g. K.; Dulebohn, J. I.; Ward, D. L.; Nocera, D. G. *Inorg. Chem.* **1996**, *35*, 811−817. For [L^{Δ}-Zn] complex, see text.

Supporting Information Available: Energies of the frontier MOs of $[L^{\Delta}Zn(CH_3CN)]$, cyclic voltammetry of the $[L^{\Delta\Delta}Zn]^{2+}/[L^{\Delta}Zn]$ redox couple, tables of crystal data, atomic coordinates, bond lengths and angles, anisotropic thermal parameters, and hydrogen coordinates for $[L^{\Delta}Zn(CH_3CN)]\cdot CH_2Cl_2$, and an X-ray crystallographic file for $[L^{\Delta}Zn(CH_3CN)]\cdot CH_2Cl_2$ in CIF format. This material is available free of charge via the Internet at http://pubs.acs.org.

JA039617H